

Estimating Cloth Elasticity Parameters Using Position-Based Simulation of Compliant Constrained Dynamics

EGOR LARIONOV, Meta Reality Labs Research, USA

MARIE-LENA ECKERT, Meta Reality Labs Research, Switzerland

KATJA WOLFF, Meta Reality Labs Research, Switzerland

TUUR STUYCK, Meta Reality Labs Research, USA

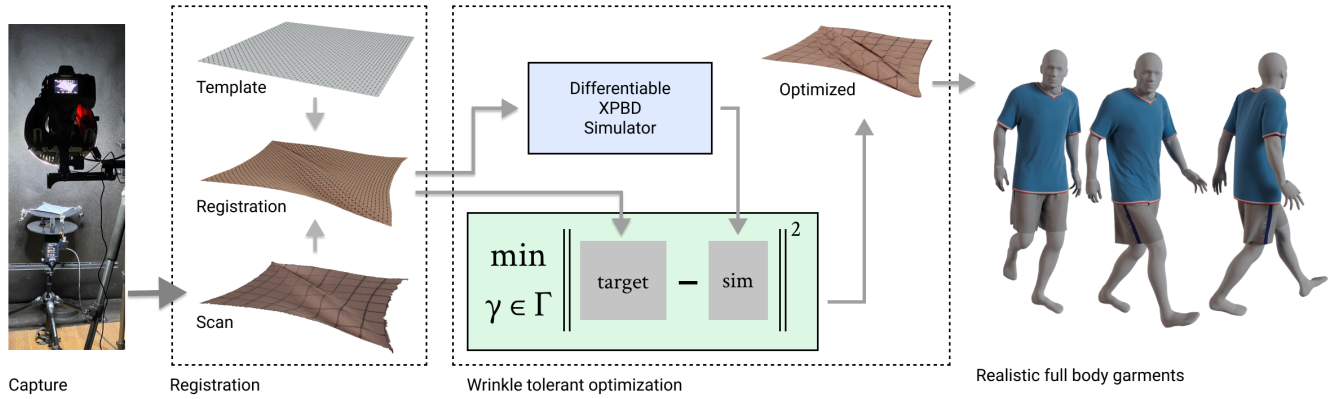


Fig. 1. *Parameter estimation pipeline.* With our pipeline, we decouple the cloth capture (left) from the parameter optimization (middle-right) using NR-ICP mesh registration (middle-left). The optimization pass is able to handle wrinkled cloth, which greatly simplifies the capture process. With the optimized parameters γ , we generate realistic full-body cloth simulation (right) bypassing laborious manual parameter picking.

Clothing plays a vital role in real life and hence, is also important for virtual realities and virtual applications, such as online retail, virtual try-on, and real-time digital avatar interactions. However, choosing the correct parameters to generate realistic clothing requires expert knowledge and is often an arduous manual process. To alleviate this issue, we develop a pipeline for automatically determining the static material parameters required to simulate clothing of a particular material based on easily captured real-world fabrics. We use differentiable simulation to find an optimal set of parameters that minimizes the difference between simulated cloth and deformed target cloth. Our novel well-suited loss function is optimized through non-linear least squares. We designed our objective function to capture material-specific behavior, resulting in similar values for different wrinkle configurations of the same material. While existing methods carefully design experiments to isolate stretch parameters from bending modes, we embrace that stretching fabrics causes wrinkling. We estimate bending first, given that membrane stiffness has little effect on bending. Furthermore, our pipeline decouples the capture method from the optimization by registering a template mesh to the scanned data. These choices simplify the capture system and allow for wrinkles in scanned fabrics. We use a differentiable extended position-based dynamics (XPBD) cloth simulator, which is capable of real-time simulation. We demonstrate our method on captured data of three different real-world fabrics and on three digital fabrics produced by a third-party simulator.

CCS Concepts: • **Computing methodologies** → **Physical simulation.**

Additional Key Words and Phrases: cloth simulation, parameter estimation

Authors' addresses: Egor Larionov, Meta Reality Labs Research, USA; Marie-Lena Eckert, Meta Reality Labs Research, Switzerland; Katja Wolff, Meta Reality Labs Research, Switzerland; Tuur Stuyck, Meta Reality Labs Research, USA.

1 INTRODUCTION

Clothing plays an important part in human culture and self-expression. The fashion industry is massive with a total worth of roughly 1.5 trillion US dollars that is even expected to double by 2025. Traditional fashion houses are becoming more and more aware of the virtual landscape and are experimenting with virtual collections in the metaverse in addition to real-world fashion lines and virtual try-on. Virtual clothing items have reduced production costs and time to market. To reproduce familiar experiences and opportunities for self-expression in the virtual world, it would be beneficial to be able to simulate a large variety of different types of clothing made from vastly different materials and structures. Unfortunately, creating realistic clothed human animations currently involves hours of tweaking simulation parameters and expert knowledge to obtain the desired clothing look. With this project, we aim to reduce the time and cost required to create realistic cloth simulations of real-world materials. While much of the effort in building simulators targets increasing numerical accuracy and minimizing computation time, we instead focus on improving the realism of an existing real-time cloth simulation method. To that end, we are the first to present a material estimation pipeline leveraging differentiable position-based simulation of compliant constrained dynamics [Macklin et al. 2016] and easy to reproduce cloth captures. Capturing cloth samples is often difficult to control due to environmental, material shape memory, and hysteresis effects. Small perturbations can lead to significantly different cloth equilibrium states, which typically makes

the optimization heavily biased towards the specific captured sample of the fabric. To overcome these limitations we introduce the following contributions:

- A novel robust objective function that operates in frequency space and is able to capture material-specific behavior, independent of the current cloth wrinkle state.
- A simplified pipeline for estimating static cloth material properties that is decoupled from the real-world capture system through a template registration process.
- A real-world validation of XPBD cloth simulation with numerical comparisons of simulated results and captured scans.
- A set of material parameters for the standard St. Venant-Kirchhoff (StVK) cloth material model for three distinct common materials.

2 RELATED WORK

Given the high relevance of virtual textile simulation both in research and manufacturing, material estimation has been a topic of investigation in the research community [Luible 2008] and industry [Browzwear 2022; CLO 3D 2022; Optitex 2022]. We highlight relevant work.

Material Parameter Estimation has been a focus point in computer graphics. While some techniques address the full scope of dynamic simulation parameters using video sequences [Bhat et al. 2003], we focus instead on elasticity, which can be inferred from static captures of deformed cloth. Wang et al. [2011] have proposed a non-standard piecewise material model and fit 39 parameters to a set of sparse correspondences. While sophisticated, their scheme can exhibit unlikely Poisson’s ratios below zero or above 0.5. Prior work focusing on mass-spring and diagonalized StVK models [Miguel et al. 2012] produce promising parameter estimations, but at the cost of requiring a complex and expensive capture setup. Furthermore, their method omits the Poisson effect, which greatly limits the applicability of their results in modern cloth simulators. Both works employ nodal positions to estimate approximation error, which makes their methods sensitive to wrinkles in captured data. Clyde et al. [2017] propose a more sophisticated non-linear material model to better fit existing standard ASTM measurements in large deformation scenarios. In contrast, we focus on improving the optimization method to handle data coming from non-standard and potentially cheaper setups. A different line of work attempts to estimate cloth simulation parameters using neural networks from a static drape [Ju and Choi 2020] or from videos [Yang et al. 2017].

Differentiable Simulation and System Identification has been investigated in recent research [Liang et al. 2019; Qiao et al. 2020] to infer material parameters from observations [Du et al. 2021; Hu et al. 2019; Jatavallabhula et al. 2021; Strecke and Stückler 2021]. Another topic of focus has been bringing real objects into the virtual world using sparse observations and interaction of the object with its environment [Chen et al. 2022; Weiss et al. 2020].

Cloth simulation has been a topic of research in computer graphics for many decades. Starting from the earlier work [Baraff and Witkin 1998], many improvements have been proposed to increase accuracy, stability and performance [Bouaziz et al. 2014; Liu

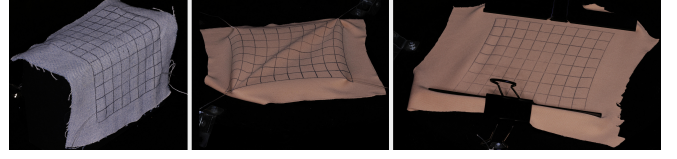


Fig. 2. *Cloth capture.* Our simple cloth capture system records the cloth swatch under different force applications to drive the optimization.

et al. 2013; Macklin et al. 2016; Müller et al. 2007; Overby et al. 2017; Stuyck 2018].

In summary, the research field has made great progress while several issues still remain. Deeply intertwined pipelines of closely coupled capture and optimization systems complicate the combination of different capture and optimization techniques. Furthermore, multiple prior works use complex capture setups that are difficult to scale. The use of absolute positions in the objective function and combined bifurcation in bending produce numerous local minima, which leads to possibly various valid configurations for the same material. Moreover, many techniques are difficult to generalize to other solvers, because they employ non-standard material models [Clyde et al. 2017; Wang et al. 2011]. In this work, we leverage position-based simulation of compliant dynamics, often referred to as *XPBD* [Macklin et al. 2016], see Section 3.3.

3 METHOD

Our goal is to estimate the material properties needed for the cloth simulator to represent particular cloth materials as realistically as possible. To achieve this, we develop a pipeline with three independent stages made from four components as visualized in Fig. 1. Initially, a *capture system* gathers point or mesh data of a deformed rectangular cloth swatch in various configurations. Then, a template mesh is *registered* to the captured data using a landmark registration technique: the non-rigid iterative closest point (NR-ICP). Finally, the registered mesh is compared to a *simulation* of the template mesh, and an optimal set of parameters is found to align both as closely as possible by using *least squares optimization*.

3.1 Capture System

We propose a lightweight cloth capture setup that can be easily reproduced with minimal cost. Cloth swatches are suspended using clamps that apply a controllable external force through weights, see Figure 2. The images are processed using *Agisoft Metashape* [Agisoft 2022] to produce a high-resolution texture mapped 3D mesh. A free and open-source alternative is *Meshroom* [Griwodz et al. 2021]. The swatch is stamped with a regular grid pattern to provide landmarks for the registration process described below.

3.2 Template Registration

In contrast to prior research, our simulation targets are decoupled from the captured scans through mesh registration, see Figure 3. We create a triangulated regular grid mesh representing the simulated cloth swatch. This template is then registered to the scan by pairing vertices of the grid with landmarks on the scanned mesh via the NR-ICP method [Li et al. 2008]. Vertices that are not aligned

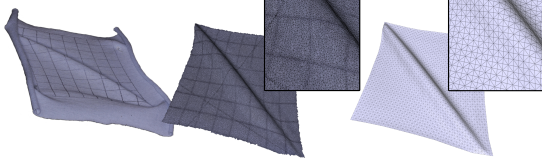


Fig. 3. *Registration.* Capture setup (left), scanned mesh (middle), and registered mesh (right) with magnified regions in the insets.

with the stamped grid pattern are projected along the mesh normal towards the surface of the scanned mesh to improve the position estimate in the normal direction. While more accurate methods have been developed for establishing dense correspondences between meshes, we stress that any stage of our pipeline – including template registration – is loosely coupled and can be replaced independently.

3.3 Simulation

XPBD is a recent constraint-based simulation model that often obtains much better performance compared to expensive non-linear solvers. It uses an iterative Gauss-Seidel solution for the linearized equations of motion. The method can be easily parallelized [Frat-cangeli et al. 2016] and implemented on hardware such as multi-core CPUs and GPUs, enabling interactive or real-time simulations on common modern hardware.

The method aims to solve Newton’s equations of motion

$$\mathbf{M}\ddot{\mathbf{x}} = -\nabla U(\mathbf{x}), \quad (1)$$

where $\mathbf{x} \in \mathbb{R}^{3n}$ encodes n vertex positions (of the cloth mesh in this case) and \mathbf{M} is the mass matrix computed from element volumes and constant material density ρ . The energy potential $U(\mathbf{x})$ needs to be specified in terms of a vector of constraint functions $\mathbf{C} = [C_1(x), C_2(x), \dots, C_m(x)]^\top$ as

$$U(\mathbf{x}) = \frac{1}{2} \mathbf{C}(\mathbf{x})^\top \boldsymbol{\alpha}^{-1} \mathbf{C}(\mathbf{x}), \quad (2)$$

where $\boldsymbol{\alpha}$ is a block diagonal compliance matrix. Any energy that can be written this way is suitable for XPBD. Using implicit Euler time integration, the XPBD algorithm reduces to solving for the constraint multiplier updates $\Delta\lambda$ with

$$(\nabla \mathbf{C}(\mathbf{x}_i)^\top \mathbf{M}^{-1} \nabla \mathbf{C}(\mathbf{x}_i) + \tilde{\boldsymbol{\alpha}}) \Delta\lambda = -\mathbf{C}(\mathbf{x}_i) - \tilde{\boldsymbol{\alpha}} \lambda_i, \quad (3)$$

where $\tilde{\boldsymbol{\alpha}} = \frac{\boldsymbol{\alpha}}{\Delta t^2}$, followed by a position update

$$\Delta \mathbf{x} = \mathbf{M}^{-1} \nabla \mathbf{C}(\mathbf{x}_i) \Delta\lambda. \quad (4)$$

The system in Eq. 3 is typically solved using Gauss-Seidel- or Jacobi-style updates.

3.3.1 Elasticity Model. We employ an orthotropic StVK membrane energy model along with simple discrete bending [Bender et al. 2017] for modelling cloth. This model suggests a per-element inverse compliance matrix of the form

$$\boldsymbol{\alpha}_\Delta^{-1} = A \begin{bmatrix} C_{00} & C_{01} \\ C_{01} & C_{11} \\ & & C_{22} \end{bmatrix},$$

where A is the area of a single triangle and C_{ij} are the compliance coefficients. The constraint function for each triangle is then defined

to be the Green strain ϵ in Voigt notation

$$\mathbf{C}_\Delta(\mathbf{x}) = (\epsilon_{uu}, \epsilon_{vv}, 2\epsilon_{uv})^\top, \quad (5)$$

where subscripts u and v indicate warp and weft directions, respectively. With orthotropic Young’s moduli E_u, E_v for modelling distinct warp and weft behavior of the fabric, Poisson’s ratios ν_{uv}, ν_{vu} and shear modulus μ , we have

$$\begin{bmatrix} C_{00} & C_{01} \\ C_{01} & C_{11} \\ & & C_{22} \end{bmatrix} = \frac{1}{1 - \nu_{uv}\nu_{vu}} \begin{bmatrix} E_u & \nu_{vu}E_u \\ \nu_{uv}E_v & E_v \\ & & \mu(1 - \nu_{uv}\nu_{vu}) \end{bmatrix}. \quad (6)$$

Note that this matrix is symmetric since $\nu_{vu}E_u = \nu_{uv}E_v$ and the Poisson’s ratio ν_{vu} corresponds to a contraction in direction u when an extension is applied in direction v . In the following sections, we abbreviate $\nu_{uv} = \nu$ whereas ν_{vu} is computed from ν, E_u , and E_v .

The bending constraint [Bender et al. 2017] is defined for each pair of adjacent triangles $(\mathbf{x}_1, \mathbf{x}_3, \mathbf{x}_2), (\mathbf{x}_1, \mathbf{x}_2, \mathbf{x}_4)$ as the angle strain

$$C_{\text{bend}} = \arccos \left(\frac{\mathbf{x}_{2,1} \times \mathbf{x}_{3,1}}{\|\mathbf{x}_{2,1} \times \mathbf{x}_{3,1}\|} \cdot \frac{\mathbf{x}_{2,1} \times \mathbf{x}_{4,1}}{\|\mathbf{x}_{2,1} \times \mathbf{x}_{4,1}\|} \right) - \phi_0,$$

where ϕ_0 is the rest dihedral angle and $\mathbf{x}_{i,j} = \mathbf{x}_i - \mathbf{x}_j$ are edge vectors between vertices i and j . The inverse compliance matrix is then given by the scalar bending stiffness: $\boldsymbol{\alpha}_{\text{bend}}^{-1} = [b]$.

3.3.2 Differentiable Simulation. To use gradient-based optimization with this compliant constraint formulation, we compute the gradient with respect to the material parameters. Both bending energy and StVK membrane energy are differentiable. It suffices to compute the derivative of the position update in Eq. 4, which involves differentiating through Eq. 3. Derivatives are computed analytically and accumulated in tandem with the Gauss-Seidel or Jacobi iterates. We must compute $\partial \Delta \mathbf{x} / \partial \gamma$ where γ is the set of parameters we aim to recover, which we define in the next section.

3.4 Estimating Elastic Material Parameters

In this section, we describe our method for finding a set of parameters γ required to reproduce a cloth shape captured under the influence of external forces. We focus on estimating static elasticity parameters that define the stress-strain relationship. Estimating parameters that describe how cloth behaves during motion, i.e., friction or damping, remains an interesting avenue for future work.

3.4.1 Optimization problem. As output from the capture pipeline, we obtain a cloth mesh in a deformed configuration at rest. We introduce *shape descriptors* \mathbf{s} that represent the cloth’s shape in different ways as in Eq. 9. Below, $\mathbf{s}_{\text{target}}$ is used to describe the target shape. To obtain more information about the stress-strain relationship in the material and to resolve global scaling ambiguities, we additionally use force data from some of the boundary nodes. While other works have used full force vectors, we opt to capture only force magnitudes $\mathbf{f}_{\text{target}}$ to avoid the need for complex and costly setups necessary to collect accurate directional forces. We then match the corresponding shape \mathbf{s}_{sim} and boundary forces \mathbf{f}_{sim} of a simulation to the target by finding suitable material properties. In general, we can stack as many meshes as needed into \mathbf{s} and \mathbf{f} .

We optimize directly over the compliance coefficients and bending parameter by choosing the parameter set to be

$$\gamma := (C_{00}, C_{11}, C_{01}, C_{11}, b), \gamma \in \Gamma, \quad (7)$$

where Γ is a rectangular constraint set of feasible material parameter combinations. The chosen parameter set γ is a better candidate for optimization compared to Young’s moduli and Poisson’s ratio due to its good relative scaling. To penalize unrealistic Poisson’s ratios ν above 0.5, we add the following penalty

$$W_\nu = \max(0, \nu - 0.5).$$

Putting everything together forms our final optimization problem

$$\min_{\gamma \in \Gamma} \|\mathbf{r}_{\text{sim}}(\gamma) - \mathbf{r}_{\text{target}}\|^2 + s_\nu W_\nu, \quad (8)$$

where $\mathbf{r}^\top = (\mathbf{s}^\top, \mathbf{f}^\top)$ is the vector of stacked shape descriptors \mathbf{s} and boundary force magnitudes \mathbf{f} . Here, \mathbf{r}_{sim} corresponds to a simulation after N timesteps of a quasi-static XPBD solve initialized to the target vertex positions, whereas $\mathbf{r}_{\text{target}}$ are the shape descriptors and measured force magnitudes of the registered mesh as described in Section 3.2. We weigh the Poisson penalty high with $s_\nu = 1e8$. To solve Eq. 8, we employ the Ceres non-linear least squares solver [Agarwal et al. 2022].

3.4.2 Shape descriptors. Many prior methods rely on precise control over cloth swatches to measure specific parameters [Clyde et al. 2017; Miguel et al. 2012; Wang et al. 2011]. In particular, it is convenient to produce deformations that are affected by just one or a few material parameters. For instance, the bending angle in a piece of cloth, as it hangs from the edge of a table, is determined by the bending parameter while being largely insensitive to changes in other stiffness parameters. Unfortunately, it is difficult to design experiments that isolate material properties like shear stiffness and Poisson’s ratio, since cloth tends to buckle in such scenarios producing wrinkles that inherently couple bending with other parameters.

Due to the bifurcation behavior of wrinkling, deformed cloth can reach distinct equilibrium states depending on the deformation trajectory, initial conditions, and material shape memory effects. Consider Fig. 4 with a square piece of cloth pulled at opposing corners for one example of such ambiguity in stable equilibrium states. Since real-world cloth can exhibit bias towards a particular wrinkle pattern, the example cloth swatch wrinkles in the same way independent of its orientation. When the cloth is flipped upside down, the pattern flips as well from a viewer perspective. However, this ambiguity poses a challenge for parameter optimization, because such effect is difficult to capture in simulation. Simulated cloth will in this case approach the same observed wrinkle pattern due to gravity. Here, naive position-based metrics will result in a very different value for both valid cloth configurations. Another example for ambiguity is visualized in Fig. 6 where simulating the same material with varying initial conditions results in two distinct equilibrium states.

While many previous methods simply avoid wrinkles in the captured data [Clyde et al. 2017; Miguel et al. 2012; Wang et al. 2011], we instead propose a novel objective to handle such ambiguities and are able to process coupled-parameter captures, which in turn allows for simpler and more affordable capture pipelines.



Fig. 4. *Wrinkle bifurcation*: two valid cloth configurations with contrary wrinkle patterns shown from above (top) and side (bottom). The same cloth swatch is pulled with the same force at opposite corners.

As outlined above, the evaluation of the objective in Eq. 8 results in a very different value for both equilibrium states in Fig. 4 when choosing \mathbf{s} to be a stacked locator of vertex positions \mathbf{p} , although both target swatches are generated with the same material properties. In general, positional loss encoding is sensitive to small differences in the captured cloth. Thus, we developed an objective function that reports a similar error for wrinkle patterns generated by the same material. We evaluate the following shape descriptors:

$$\begin{aligned} \mathbf{s}_{\text{pos}}(\mathbf{p}) &= \mathbf{p}, \\ \mathbf{s}_{\text{energy}}(\mathbf{p}) &= \mathbf{U}_{\text{triangle}}(\mathbf{p}) + \mathbf{U}_{\text{bend}}(\mathbf{p}), \\ \mathbf{s}_{\text{strain}}(\mathbf{p}) &= \mathbf{C}_{\text{triangle}}(\mathbf{p}) + \mathbf{C}_{\text{bend}}(\mathbf{p}), \\ \mathbf{s}_{\text{FFT}}(\mathbf{p}) &= \text{FFT}(\mathbf{p}), \end{aligned} \quad (9)$$

where \mathbf{U} is either a triangle or bending *energy* and \mathbf{C} is the *strain* as defined in Section 3.3.1. The position descriptor \mathbf{s}_{pos} represents the swatch shape in terms of vertex positions, leading to evaluating the absolute position of wrinkles. In contrast, $\mathbf{s}_{\text{energy}}$ and $\mathbf{s}_{\text{strain}}$ measure the per-element energies and strain, respectively, which determine how much the cloth is stretched. They differ in \mathbf{U} usually being a squared strain scaled by the material parameters. This implies that $\mathbf{s}_{\text{target}}$ depends on γ , which complicates the computation of the corresponding derivatives. The finite Fourier transform (FFT) descriptor \mathbf{s}_{FFT} applies the normalized 2D FFT to grid vertices. The normalization removes phase information, leading to small metric differences when comparing distinct wrinkle phases and larger discrepancies for varying wrinkle amplitude or frequency.

Our experiments show that the energy and strain descriptors $\mathbf{s}_{\text{energy}}$ and $\mathbf{s}_{\text{strain}}$ work well when bifurcations are symmetric as in Fig. 4. However, for fine wrinkles as in Fig. 5, only the FFT descriptor \mathbf{s}_{FFT} performs robustly as we elaborate in the next section.

4 EVALUATION

In this work, we use the centimetre–gram–second (CGS) system of units for material parameters. While our optimization results in optimal parameters γ as defined in Eq. 7, we often report the traditional, more intuitive parameters E_u, E_v, μ, ν instead of C_{00}, C_{11}, C_{01} , and C_{22} as defined in Eq. 6. In the following sections, we use γ to represent parameters in both forms depending on context.

A popular experiment for cloth is the *picture frame shear*. Here, a square piece of cloth is fixed on all sides onto a rigid “picture frame”, which is then deformed at the hinges. For validation purposes, we hand-pick fictional properties for three synthetic materials, see Table 1 (top), that we call cotton, denim, and silk as they produce visually similar shapes to these fabrics. We then simulate a picture frame experiment using two different initial conditions for all three materials. For this experiment we use a square cloth swatch with a

side length of 15 cm. The two initial conditions are perturbed vertex positions and a flat alignment of all vertices. The simulations with varying initial conditions converge to significantly different equilibrium states for each material as shown in Fig. 6, which demonstrates the ambiguity mentioned in Section 3.4.2.

4.1 Choice of Objective Function

To evaluate the effectiveness of the proposed shape descriptors s , we generate a synthetic cotton picture frame experiment with our XPBD simulator and γ_{cotton} , see target shape in Fig. 5. Starting with perturbed parameters $\gamma_{\text{initial},c}$ from Table 1 (middle), we optimize for material parameters with each of the four shape descriptor from Eq. 9. We then run four simulations with the found parameter sets, all initialized to the target cloth shape. As demonstrated in Fig. 5, the optimization using the parameters retrieved through the FFT descriptor s_{FFT} converges to the exact target cloth shape while s_{energy} and s_{strain} produce the largest differences to the target.

Furthermore, we assess the ability of s_{pos} and s_{FFT} to discriminate between different materials. Thereby, we evaluate both descriptors on simulations of the same material with varying initial conditions and on simulations of different materials. We want the descriptors to be similar for the first case, but divergent for the second. We evaluate cloth simulations for three materials $m \in \{\text{cotton, denim, silk}\}$ with two varying initial conditions $\{\mathbf{p}_{\text{initial}1}, \mathbf{p}_{\text{initial}2}\}$ on a cloth swatch as described in Fig. 6. The descriptor difference Δs within one material, here for FFT, is

$$\Delta s_{\text{FFT},m} = \|s_{\text{FFT},m}(\mathbf{p}_{\text{initial}1}) - s_{\text{FFT},m}(\mathbf{p}_{\text{initial}2})\|_2.$$

The delta across two different materials $m, m2$ with $m2 \in \{\{\text{cotton, denim, silk}\} \setminus m\}$ is defined as

$$\Delta s_{\text{FFT},m,m2,i,j} = \|s_{\text{FFT},m}(\mathbf{p}_i) - s_{\text{FFT},m2}(\mathbf{p}_j)\|_2,$$

with $i, j \in \{\text{initial}1, \text{initial}2\}$. Since these absolute values are not necessarily comparable across different descriptors, we instead compare relative differences:

$$\Delta \hat{s}_{\text{FFT},m,m2,i,j} = \Delta s_{\text{FFT},m,m2,i,j} - \Delta s_{\text{FFT},m},$$

where positive values indicate that the descriptor reports larger shape differences in different materials than varying cloth configurations for one material, as desired. With $m2$ and i, j , we obtain

	E_u	E_v	μ	ν	b
γ_{cotton}	1.0e5	2.8e5	4.0e4	0.4	50
γ_{denim}	5.0e5	7.0e5	2.0e4	0.45	200
γ_{silk}	2.0e5	3.0e5	1.5e4	0.35	10
$\gamma_{\text{initial},c}$	2.0e5	1.8e5	5.0e4	0.3	10
$\gamma_{\text{FFT},c}$	9.98e4	2.79e5	3.98e4	0.40	51.96

Table 1. *Material properties for validation with XPBD.* Hand-picked properties for three synthetic materials (top), perturbed initial conditions for cotton (middle), and the recovered parameter set $\gamma_{\text{FFT},c}$ (bottom) with inputs as in Fig. 8. Here, we choose high stiffness values due to finding the simulation to converge to more realistic equilibria while using larger time steps, see Section 3 in the supplemental document for details.

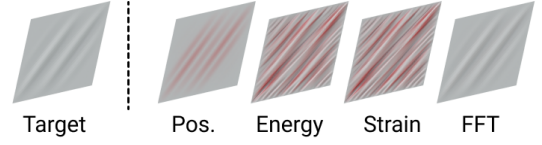


Fig. 5. *Shape descriptor evaluation.* Target cloth is simulated with XPBD (left) followed by optimization results for each descriptor (right). Euclidean vertex distances to the target are color-coded with a maximum of 1.8 mm.

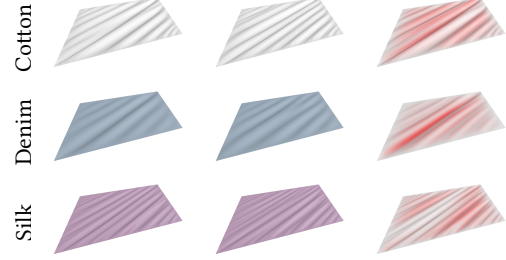


Fig. 6. *Distinct equilibrium states for the same material.* Two simulations for each material with different initial conditions: perturbed vertices (left), flat configuration (middle), and color-coded Euclidean distance between both meshes in red (right), with a maximum distance of 4.3 mm.

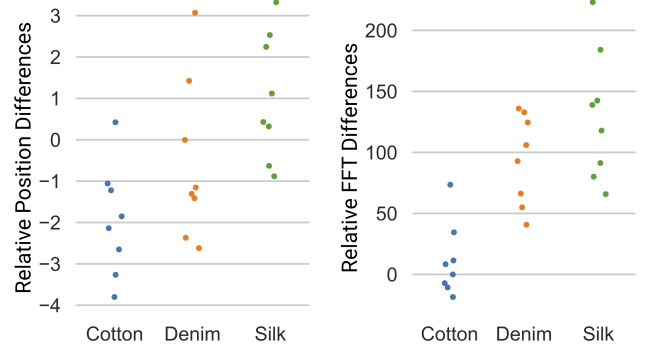


Fig. 7. *Relative metric differences.* Values of $\Delta \hat{s}_{\text{pos},m,m2,i,j}$ (left) and $\Delta \hat{s}_{\text{FFT},m,m2,i,j}$ (right) where m is the x -axis: s_{pos} doesn't necessarily produce higher metric differences across materials compared to varying cloth configurations for the same material, as shown by the negative and close-to-zero values (left), while s_{FFT} does as observed in the mostly positive values (right).

eight instances of $\Delta \hat{s}_{\text{FFT},m,m2,i,j}$ for each material m . Fig. 7 shows that the FFT shape descriptor correctly produces higher differences for varying materials compared to distinct configurations of the same material. Hence, we choose the FFT shape descriptor for our objective function.

4.2 Validation

To analyze the accuracy of our novel parameter estimation, we generate four synthetic cotton simulations with our XPBD simulator: two picture frame deformations and two stretch experiments

as visualized in Fig. 8. To allow for precise comparison of the retrieved and target parameter sets, we use the same XPBD simulator as we employ in the optimization. Starting with the same perturbed parameter set $\gamma_{\text{initial},c}$ as in the previous section, our optimizer recovers the target parameters very well after 13 iterations as shown in Table 1 (bottom) – although only four target cloth shapes are used. Remarkably, the bending parameter is recovered within a 4% error in spite of there being no explicit bending examples in the target set. The membrane parameters are recovered within 0.5% error.

In Fig. 9 we further compare the shapes of unseen cloth configurations re-simulated with our retrieved parameter set $\gamma_{\text{FFT},c}$ to target simulations created with γ_{cotton} . The error in the recovered parameters causes a difference in vertex positions below 0.28 mm, which is largely imperceptible.



Fig. 9. Re-simulation of various cloth configurations with $\gamma_{\text{FFT},c}$ estimated from XPBD targets with γ_{cotton} . The vertex displacement error is color-coded in red, with a small maximum error of 0.28 mm. The second and last columns are targets while the rest are unseen by the optimization.

5 RESULTS

Synthetic Experiments. We show that our method is capable of reproducing cloth simulations from third-party software. First, we generate a set of square swatch targets in Houdini [SideFX 2019] with different material presets; the targets for silk are depicted in Fig. 10. Then, we estimate the bending parameter b using the bending scenarios of Fig. 10 (right). The membrane parameters ($C_{00}, C_{11}, C_{01}, C_{22}$) are estimated together in a separate pass by pulling the corners of the suspended cloth swatch as in Fig. 10 (left). This process is repeated thrice to ensure that the coupling between bending and membrane stiffnesses is not lost. Furthermore, to avoid getting stuck in local minima, we run the same optimization from three different randomized starting points.

This decoupling technique produces a lower objective, i.e., a better fit, compared to optimizing all parameters at once. In the future, we aim to further eliminate the need for separate passes for bending and membrane parameters to produce a more streamlined pipeline. The comparison to Houdini silk targets is illustrated in Fig. 11. For



Fig. 10. Synthetic silk targets generated with Houdini, used for estimating membrane stiffnesses (left) and bending stiffnesses (right).



Fig. 11. Re-simulation with the estimation of Houdini's silk preset. The vertex displacement error is color-coded in red with a maximum set to 2 mm. In the second column, errors are clustered on the large stretch areas with a maximum of 6 mm while it is below 2.4 mm in the remaining columns.

all deformations apart from the second column, the local vertex displacement is below 2.4 mm. In the second column, the error is clustered at large strain regions, which indicates that our StVK model deviates from Houdini's material model for large strain deformations.

The retrieved parameters are listed in Table 2. By optimizing for these parameters, we avoid manual hand-picking of material parameters as in Section 4, but instead, are able to reproduce the cloth behavior of the physically more accurate and computationally more expensive Houdini FEM simulator as demonstrated in Fig. 12. Here, we re-simulate the Houdini experiment with our XPBD simulator by using the same initial and boundary conditions as in Houdini. We thereby demonstrate that our pipeline is capable of effectively reproducing the aesthetics of different cloth materials generated by third-party simulators.

Real-world Experiments. With real-world captures of cloth subject to various force applications and deformations, we generate six targets each for three different materials as shown in Fig. 13 using a 9.6 cm cloth swatch. The first two targets are generated by applying a 200 g weight on opposing sides of the cloth using wide paper clamps as shown in Fig. 2 (right). The third target is generated by

Material (ρ in g/cm ²)	E_u	E_v	μ	ν	b
Denim (0.0324)	34182	33735	5592	0.2609	11.0
Cotton (0.0224)	30823	30266	4971	0.3058	1.19
Silk (0.0187)	7492	7436	1193	0.03543	0.100

Table 2. Estimation of material parameters for Houdini's FEM cloth solver.

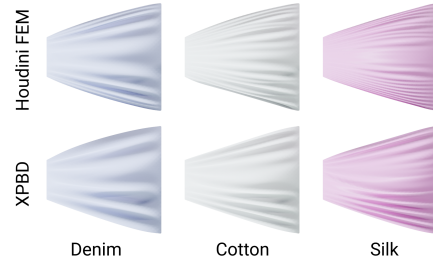


Fig. 12. Aesthetic evaluation. By twisting a piece of cloth, unseen by optimization, we demonstrate that distinct wrinkle patterns generated by Houdini's FEM simulator are reproduced using our XPBD simulator with optimized material parameters.

applying a 200 g weight on all corners while the fourth is created by applying 20 g at two diagonally opposite corners and 100 g on the remaining corners. The last two targets are generated by letting the cloth drape from a horizontal ledge.

We optimize for the parameters of each material, which are shown in Table 3. Then, we re-simulate the target with the estimated parameters by setting the initial vertex positions to the target shapes, see Fig. 14. Our results demonstrate that our method is able to closely match the captured targets within 3.7 mm of maximum vertex displacement. Our optimization correctly determines higher Young’s moduli for a stiff material like denim and lower for the softer polyester material, as well as a larger bending stiffness in denim compared to cotton and polyester.

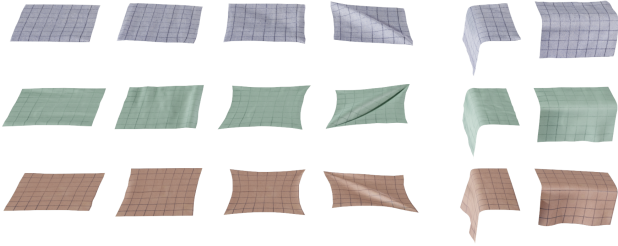


Fig. 13. *Real-world targets.* A piece of denim (top), cotton (middle), and polyester (bottom) is deformed in various configurations. The target meshes are generated through template registration as described in Section 3.2.

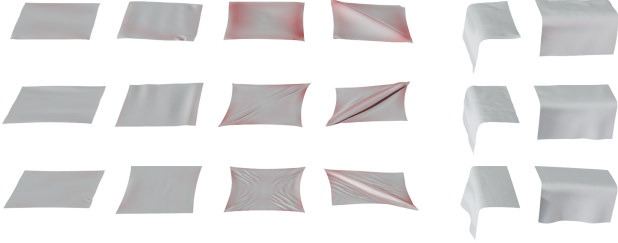


Fig. 14. *Real-world results.* Denim (top), cotton (middle), and polyester (bottom) cloth is simulated with our estimated parameters. The vertex position error to the targets in Fig. 13 is colored in red with a maximum of 3.7 mm.

Material (ρ in g/cm ²)	E_u	E_v	μ	ν	b
Denim (0.0324)	3793	20590	6968	0.4286	28.5
Cotton (0.0224)	1840	2019	6538	0.4308	8.99
Polyester (0.0187)	1028	3271	9171	0.2731	2.35

Table 3. *Estimation of material parameters for real-world targets.*

Note that the stiffness parameters in Table 3 are lower than in Table 2, since the forces applied on the boundary are smaller in the real-world case, e.g., 0.2 Mdyn vs. 3 Mdyn, which leads to a similar amount of strain. As our method aims at small strain deformations, we expect to see lower stiffness estimates. However, we plan to

extend our analysis to more sophisticated large strain models, and experiment with larger forces for captured data in the future.

To further validate that our results produce the desired look, we simulate full outfits using the estimated parameters in Fig. 15.

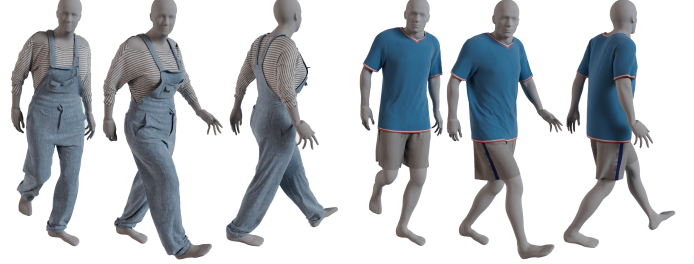


Fig. 15. *Outfit simulation:* a denim overall and cotton top (left) and a polyester soccer outfit (right).

6 LIMITATIONS AND FUTURE WORK

We presented a novel approach to cloth captures and optimization that simplifies the inverse design problem of parameter estimation. Despite improving robustness and simplicity over prior work, several limitations remain. For instance, the accuracy of our template registration technique is limited to the resolution of the stamped pattern. Additionally, as is common with non-linear optimization, our system is sensitive to objective scaling even with our FFT metric, and heuristics are required to establish a reasonable scaling between the shape descriptor metric and the force metric.

As part of future work, we aim to implement the method on GPUs to optimally leverage available compute resources and to greatly speed up to optimization time. Additionally, we intend to extend our research to different material models such as piece-wise constant stiffnesses for a piece-wise linear elastic model [Wang et al. 2011] or the Stable Neo-Hookean model for volumetric simulations [Macklin and Muller 2021]. Research into perceptual or feature-based cloth quality metrics offers the potential to further embrace the inherent coupling of cloth material parameters.

Our method uses a constant simulation time to reach equilibrium. While time to equilibrium is generally short close to the optimum, we can expect it to increase when initial parameters are chosen poorly. We plan to use adaptive simulation times in the future, which will further improve the robustness of our estimates.

7 CONCLUSION

We have presented a novel, simple pipeline to capture, register, and optimize for cloth material parameters using a simulation engine. Our proposed pipeline consists of three separate stages that can be improved upon individually. We proposed a novel metric that enables us to capture coupled cloth shearing, stretching, and bending effects, which in turn allows for more efficient and easier capture setups. Our material parameters are not limited to the XPBD framework and can be reused with different simulation techniques that employ the same material model.

ACKNOWLEDGMENTS

We would like to thank Michelle Hill and Arkell Rasiah for their help with the cloth captures.

REFERENCES

- Sameer Agarwal, Keir Mierle, and Others. 2022. Ceres Solver. <http://ceres-solver.org>. Agisoft. 2022. Agisoft Metashape.
- David Baraff and Andrew Witkin. 1998. Large steps in cloth simulation. In *Proceedings of the 25th annual conference on Computer graphics and interactive techniques*. 43–54.
- Jan Bender, Matthias Müller, and Miles Macklin. 2017. A Survey on Position Based Dynamics, 2017. In *EUROGRAPHICS 2017 Tutorials*. Eurographics Association.
- Kiran S. Bhat, Christopher D. Twigg, Jessica K. Hodgins, Pradeep K. Khosla, Zoran Popović, and Steven M. Seitz. 2003. Estimating Cloth Simulation Parameters from Video. In *Proceedings of the 2003 ACM SIGGRAPH/Eurographics Symposium on Computer Animation* (San Diego, California) (SCA '03). Eurographics Association, Goslar, DEU, 37–51.
- Sofien Bouaziz, Sebastian Martin, Tiantian Liu, Ladislav Kavan, and Mark Pauly. 2014. Projective dynamics: Fusing constraint projections for fast simulation. *ACM transactions on graphics (TOG)* 33, 4 (2014), 1–11.
- Browzwear. 2022. Browzwear Fabric Analyzer. <https://browzwear.com/products/fabric-analyzer/>.
- Hsiao-yu Chen, Edgar Tretschk, Tuur Stuyck, Petr Kadlec, Ladislav Kavan, Etienne Vouga, and Christoph Lassner. 2022. Virtual Elastic Objects. *arXiv preprint arXiv:2201.04623* (2022).
- CLO 3D. 2022. CLO. <https://www.clo3d.com/>.
- David Clyde, Joseph Teran, and Rasmus Tamstorf. 2017. Modeling and Data-Driven Parameter Estimation for Woven Fabrics. In *Proceedings of the ACM SIGGRAPH / Eurographics Symposium on Computer Animation* (Los Angeles, California) (SCA '17). Association for Computing Machinery, New York, NY, USA, Article 17, 11 pages. <https://doi.org/10.1145/3099564.3099577>
- Tao Du, Kui Wu, Pingchuan Ma, Sebastian Wah, Andrew Spielberg, Daniela Rus, and Wojciech Matusik. 2021. DiffPD: Differentiable Projective Dynamics with Contact. *arXiv preprint arXiv:2101.05917* (2021).
- Marco Fratarcangeli, Valentina Tibaldo, and Fabio Pellacini. 2016. Vivace: A practical gauss-seidel method for stable soft body dynamics. *ACM Transactions on Graphics (TOG)* 35, 6 (2016), 1–9.
- Carsten Griwodz, Simone Gasparini, Lilian Calvet, Pierre Gurdjos, Fabien Castan, Benoit Maujean, Gregoire De Lillo, and Yann Lanthony. 2021. AliceVision Meshroom: An open-source 3D reconstruction pipeline. In *Proceedings of the 12th ACM Multimedia Systems Conference - MMSys '21*. ACM Press. <https://doi.org/10.1145/3458305.3478443>
- Yuanming Hu, Jiancheng Liu, Andrew Spielberg, Joshua B Tenenbaum, William T Freeman, Jiajun Wu, Daniela Rus, and Wojciech Matusik. 2019. ChainQueen: A Real-Time Differentiable Physical Simulator for Soft Robotics. *Proceedings of IEEE International Conference on Robotics and Automation (ICRA)* (2019).
- Krishna Murthy Jatavalabhula, Miles Macklin, Florian Golemo, Vikram Voleti, Linda Petrini, Martin Weiss, Breandan Considine, Jerome Parent-Levesque, Kevin Xie, Kenny Erleben, Liam Paull, Florian Shkurti, Derek Nowrouzezahrai, and Sanja Fidler. 2021. gradSim: Differentiable simulation for system identification and visuomotor control. *International Conference on Learning Representations (ICLR)* (2021). https://openreview.net/forum?id=c_E8kFWfhp0
- Eunjung Ju and Myung Geol Choi. 2020. Estimating Cloth Simulation Parameters From a Static Drape Using Neural Networks. *IEEE Access* 8 (2020), 195113–195121.
- Hao Li, Robert W Sumner, and Mark Pauly. 2008. Global correspondence optimization for non-rigid registration of depth scans. In *Computer graphics forum*, Vol. 27. Wiley Online Library, 1421–1430.
- Junbang Liang, Ming Lin, and Vladlen Koltun. 2019. Differentiable Cloth Simulation for Inverse Problems. In *Advances in Neural Information Processing Systems*, H. Wallach, H. Larochelle, A. Beygelzimer, F. d'Alché-Buc, E. Fox, and R. Garnett (Eds.), Vol. 32. Curran Associates, Inc. <https://proceedings.neurips.cc/paper/2019/file/28f0b864598a1291557bed248a998d4e-Paper.pdf>
- Tiantian Liu, Adam W Bargteil, James F O'Brien, and Ladislav Kavan. 2013. Fast simulation of mass-spring systems. *ACM Transactions on Graphics (TOG)* 32, 6 (2013), 1–7.
- Christiane Luible. 2008. *Study of mechanical properties in the simulation of 3D garments*. Ph. D. Dissertation. University of Geneva.
- Miles Macklin and Matthias Muller. 2021. A Constraint-based Formulation of Stable Neo-Hookean Materials. In *Motion, Interaction and Games*. 1–7.
- Miles Macklin, Matthias Müller, and Nuttapong Chentanez. 2016. XPBD: position-based simulation of compliant constrained dynamics. In *Proceedings of the 9th International Conference on Motion in Games*. 49–54.
- E. Miguel, D. Bradley, B. Thomaszewski, B. Bickel, W. Matusik, M. A. Otaduy, and S. Marschner. 2012. Data-Driven Estimation of Cloth Simulation Models. *Computer Graphics Forum* 31, 2pt2 (2012), 519–528. <https://doi.org/10.1111/j.1467-8659.2012.03031.x> arXiv:<https://onlinelibrary.wiley.com/doi/pdf/10.1111/j.1467-8659.2012.03031.x>
- Matthias Müller, Bruno Heidelberger, Marcus Hennix, and John Ratcliff. 2007. Position based dynamics. *Journal of Visual Communication and Image Representation* 18, 2 (2007), 109–118.
- Optitex. 2022. Optitex Fabric Analyzer. <https://optitex.com/products/fabric-management/>.
- Matthew Overby, George E Brown, Jie Li, and Rahul Narain. 2017. *IEEE Transactions on Visualization and Computer Graphics* 23, 10 (2017), 2222–2234.
- Yi-Ling Qiao, Junbang Liang, Vladlen Koltun, and Ming C. Lin. 2020. Scalable Differentiable Physics for Learning and Control. In *ICML*.
- SideFX. 2019. Houdini.
- Michael Strecke and Jörg Stückler. 2021. DiffSDFS: Differentiable Rigid-Body Dynamics With Implicit Shapes. In *International Conference on 3D Vision (3DV)*.
- Tuur Stuyck. 2018. Cloth Simulation for Computer Graphics. *Synthesis Lectures on Visual Computing: Computer Graphics, Animation, Computational Photography, and Imaging* 10, 3 (2018), 1–121.
- Huamin Wang, James F O'Brien, and Ravi Ramamoorthi. 2011. Data-driven elastic models for cloth: modeling and measurement. *ACM transactions on graphics (TOG)* 30, 4 (2011), 1–12.
- S. Weiss, R. Maier, D. Cremers, R. Westermann, and N. Thuerey. 2020. Correspondence-Free Material Reconstruction using Sparse Surface Constraints. In *Conference on Computer Vision and Pattern Recognition (CVPR)*. Seattle, WA, USA.
- Shan Yang, Junbang Liang, and Ming C Lin. 2017. Learning-based cloth material recovery from video. In *Proceedings of the IEEE International Conference on Computer Vision*. 4383–4393.